Electric-field-controlled unpinning of scroll waves

Zulma A. Jiménez, Zhihui Zhang, and Oliver Steinbock
Florida State University, Department of Chemistry and Biochemistry, Tallahassee, Florida 32306-4390, USA
(Received 23 August 2013; published 27 November 2013)

Three-dimensional excitation vortices exist in systems such as chemical reactions and the human heart. Their one-dimensional rotation backbone can pin to unexcitable heterogeneities, which greatly affect the structure, dynamics, and lifetime of the vortex. In experiments with the Belousov-Zhabotinsky reaction, we demonstrate vortex unpinning from a pair of inert and impermeable spheres using externally applied electric fields. Unpinning occurs abruptly but is preceded by a slow reorientation and deformation of the initially circular vortex loop. Our experimental findings are reproduced by numerical simulations of an excitable reaction-diffusion-advection model.

DOI: 10.1103/PhysRevE.88.052918 PACS number(s): 05.45.−a, 82.40.Ck, 82.40.Qt

I. INTRODUCTION

Living systems utilize excitable and oscillatory dynamics to orchestrate a wealth of functions requiring clock-like behavior, macroscopic patterns, and long-range communication [1]. Important examples include circadian rhythms [2], morphogenesis-controlling concentrations fields [3], neuronal communication [4], neural representations [5], and cardiac dynamics [6]. Despite the robustness and versatility of the underlying nonlinear phenomena, they can also become the source of dynamic diseases. Two well-known examples are epileptic seizures [7], in which large numbers of neurons synchronize their activity patterns, and cardiac arrhythmias, such as tachycardia and fibrillation [6,8]. The latter, life-threatening conditions are closely related to reentrant electrical waves that create rhythmic—or chaotic—dynamics with frequencies much higher than the normal heart beat [8,9].

It has long been recognized that tachycardia and fibrillation are the result of vortex-like activation patterns that in the thick ventricles of the human heart require a three-dimensional description [10–13]. In the realm of nonlinear physics and complexity research, such three-dimensional patterns are known as scroll waves [13–15]. They rotate around one-dimensional phase singularities and, if obtained in the normal direction to these filaments, any two-dimensional cross-section reveals locally rotating spiral waves [16]. In the limit of low curvature and twist, the motion of an unperturbed, free filament depends on its local curvature K and two system parameters, α and β, which themselves depend in a very complicated fashion on the underlying reaction-diffusion equations. The parameter α is known as the filament tension and affects the velocity v_N in the normal direction to the filament according to $v_N = -\alpha K$. For $\alpha > 0$, filament loops shrink, converge to circles, and eventually annihilate [17]; for $\alpha < 0$, filament loops expand and induce scroll wave turbulence [18]. The parameter β affects the speed v_B in the binormal direction according to $v_B = \beta K$. Both parameters can be readily measured from the dynamics of scroll rings with circular filaments (see, e.g., Ref. [19]).

Scroll waves are also found in aggregating slime molds [20] and in the autocatalytic Belousov-Zhabotinsky (BZ) reaction [21]. The latter system continues to serve as a simple experimental model for the study of vortex states in living matter as well as a motivational source for theoretical work on excitable reaction-diffusion systems. Despite the numerous similarities between the BZ reaction and biological systems, there are also important differences; for instance, cardiac tissue is, in contrast to the BZ reaction, anisotropic and spatially heterogeneous. In addition, the heart responds to increased action potentials with muscular contraction and vice versa mechanical perturbations can alter the heart's electric state [22,23].

The heterogeneous nature of the heart is not limited to presence of cells and subcellular structures but extends, in the form of blood vessels and remodeled myocardium [24], to macroscopic length scales. Remodeled myocardium forms after traumatic events, such as myocardial infarction, and contains large numbers of unexcitable myofibroblasts and reduced concentrations of the gap junction protein Connexin43 [25,26]. This "scar tissue" shows contractile dysfunction and slow conduction due to the resulting changes in intracellular coupling that in a core region could block pulse propagation. Remodeled myocardium also plays an important role in the pathogenesis of ventricular tachycardia after infarction. Recent studies suggest that it increases the inducibility of tachycardia and acts in an arrhythmogenic fashion but decreases the reentrance frequency during the arrhythmia [24–26]. At least the latter observation can be interpreted as the consequence of more expansive vortex rotation around regions of reduced excitability.

These poorly understood and complex dependencies prompted us to investigate the interaction of scroll waves and unexcitable heterogeneities in isotropic model systems [27,28]. Recent results revealed a variety of unexpected phenomena, including the self-wrapping of filaments around cylindrical wave obstacles [29] and the creation of stationary gradients in rotation phase (twist) [30]. Furthermore, we showed that the curvature-induced shrinking of filament loops can be stopped by local pinning to two or more inert spheres [31,32]. All of these studies demonstrate that heterogeneities dramatically affect the structure and the lifetime of vortex states. Furthermore, pinning is readily accomplished and robust against a wide variety of changes in the filament shape, the initial condition, and the size and shape of the heterogeneity. Here, we show that—despite this robustness—scroll waves can be unpinned by externally applied fields.

II. EXPERIMENTAL

Our experiments use the ferroin-catalyzed BZ reaction, which is an excitable reaction-diffusion medium. The system is composed of two gel layers (0.8% w/v agar). Both layers measure 4 mm in thickness and contain—within the experimental error—a reaction medium of identical, initial concentrations. Disregarding the bromination of malonic acid, these concentrations are $[NaBrO_3] = 0.04$ mol/L, [malonic acid] = 0.04 mol/L, $[H_2SO_4] = 0.16$ mol/L, and $[Fe(phen)_3SO_4] = 0.5$ mmol/L. Notice that our earlier studies [29–32] employed a liquid BZ layer on top of a BZ gel; however, a liquid BZ layer is still used during the initiation phase of the scroll wave as described below.

During the gelation process of the lower layer, we place two glass beads (radius 1.0 mm) onto the forming gel surface and gently press them halfway into the medium. After completion of gelation, we add BZ solution (same concentration as above) onto the gel and initiate a nonrotating, nearly spherical chemical wave using the tip of a vertically oriented silver wire. The mechanism behind the silver-mediated wave nucleation is the formation of insoluble silver bromide, which decreases the local concentration of dissolved, inhibitory bromide ion. The wave is started at the point located halfway between the two beads. The system is then manually swirled to create a homogeneous, upper layer. Notice that this motion does not affect the expansion of the half-spherical wave in the gel. The main purpose of the liquid layer is to minimize the inflow of inhibitory molecular oxygen from the atmosphere as well as other undesired mass transport between the reaction system and the ambient air. Once the wave reaches the beads, we decant the liquid into a waste container and replace it with a solution containing the BZ reagents and agar. This solution is at a temperature slightly above the gelling point (36–40 °C) and gels within 1–2 min. Then we place a flat glass plate onto the system to prevent the inflow of oxygen. After creation of the upper gel layer, the rim of the half-spherical wave in the lower part now curls upwards and nucleates the desired scroll ring. Moreover, the filament of the scroll ring is pinned to both beads.

During the latter stages, we also connect the reaction system to two plate-like electrodes that allow us to carry out the unpinning experiments. The two electrodes consist of copper plates (80 mm long, 20 mm wide, and 0.25 mm thick) and are connected to a regulated DC power supply (TexPower, HY3003D). They are inserted into the gel at a relative distance of 10 cm from each other with the scroll ring and beads nearly centered. Typical voltages applied in our experiments range between 5 and 25 V. To compensate for Ohmic heating, we thermally connect the system to a large, unstirred water bath. For the highest field strengths of $E = 2$–2.5 V/cm, the temperature during the experiments revealed a tolerable increase of only 2 °C over the course of 1–2 h. Various unidentified reaction products form at the electrodes; however, the maximal duration of our measurements (2 h) is too short to allow for diffusive influx into the main area of interest.

The reaction system is illuminated by white light and monitored using a charge-coupled-device camera (COHU, 2122-1000) equipped with a blue dichroic filter (Edmund Optics, 90% transmission from 400 to 500 nm). The camera signal is digitized using a PC-based frame grabber board (Data Translation DT-3155) and HL-Image-97++ software. Image analysis is carried out using in-house MATLAB scripts.

As reported earlier [29], the given BZ system has a filament tension of $\alpha = +(1.4 \pm 0.2) \times 10^{-5}$ cm^2/s and accordingly free filaments show curve-shrinking dynamics rather than scroll wave turbulence. The drift coefficient β equals zero within the experimental error. Free filament movement in the binormal direction is hence negligible and planar filament loops should not move out of their initial plane as long as twist and other noncurvature effects are small.

III. RESULTS AND DISCUSSION

Figures 1(a)–1(f) show still images of scroll waves in our three-dimensional BZ medium. The data are obtained by a camera mounted above the reaction system and hence local intensities correspond to the light transmitted along 8-mm-long vertical paths. Bright and dark areas indicate overall high and low concentrations of the oxidized catalyst (ferriin), respectively. Steep and smooth gradients in the gray levels suggest wave fronts and wave backs, respectively. The two brightest spots in each frame are the glass beads that act as pinning sites of the reaction-diffusion vortices. Figures 1(a), 1(c), and 1(e) are snapshots of the fully formed scroll waves prior to electric-field perturbation. The filament

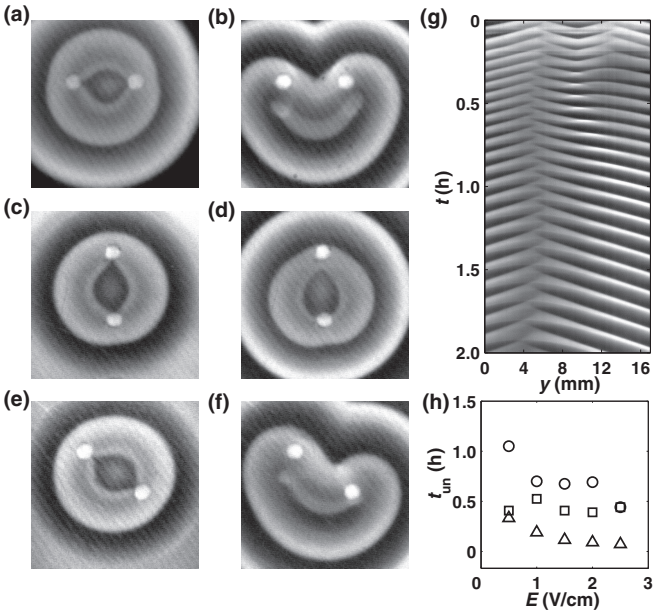

FIG. 1. (a)–(f) Still frames of scroll rings prior to (a), (c), (e) and after (b), (d), (f) electric-field controlled unpinning. The three experiments differ only in the angle ϑ between the bead-to-bead axis and the externally applied electric field: $\vartheta = 90°$ (a), (b), 0° (c), (d), and 45° (e), (f). Notice that electric field (1.5 V/cm) points downwards in all six still frames (a)–(f). Time between images: 45 min between (a) and (b); 8 min between (c) and (d); 47 min between (e) and (f). Image area for (a)–(f): 20×20 mm^2. (g) Space-time plot for the experiment shown in (a), (b) obtained along the vertical line halfway between the spheres. (h) Time t_{un} needed to remove the vortex from at least one bead as a function of the electric field strength. Circles, triangles, and squares represent data from experiments with $\vartheta = 90°$, 0°, and 45°, respectively.

loop of each vortex is pinned to the bead pair and traces a lens-shaped curve. Without the pinning sites (and in the absence of an applied field), circular scroll rings, with a filament diameter equal to the interbead distance, would collapse and annihilate during the course of 14 rotation periods [19,33]. The distance between the beads, however, is large enough to establish the stationary (or at least long-lived) state shown in Figs. 1(a), 1(c), and 1(e). This state is an excellent structure for testing if and how scroll waves can be unpinned by external perturbations.

We induce filament detachment by applying an external electric field to the system. Comparable studies of quasi-2D, obstacle-free BZ systems have shown that spiral waves—the flat analog of scroll waves—drift toward the anode with a superposed and chirality-dependent, perpendicular component [34,35]. For three-dimensional media, Luengviriya *et al.* [36,37] showed that homogeneous electric fields turn free filament loops into a plane oriented normal to the electric field. In addition, the filament moves toward the anode and tends to increase in diameter. The primary molecular basis for these effects lies in the electromigration of bromide ions, which are an important inhibitory species in the BZ reaction.

Figures 1(b), 1(d), and 1(f) illustrate the behavior of pinned scroll rings in static, homogeneous electric fields $\vec{E}$. In all three examples, the field vector is oriented parallel to the vertical edge of the images pointing downwards. Notice that the bead-to-bead axis is perpendicular to $\vec{E}$ in Figs. 1(a) and 1(b), parallel in Figs. 1(c) and 1(d), and at a 45 degree angle in Figs. 1(e) and 1(f). The images reveal that all three wave patterns are strongly deformed by the applied field. In Fig. 1(b), for instance, one of the emitted wave fronts has the shape of a heart rather than an approximate circle. Within this "heart" is a U-shaped, oxidized region that contains the filament. The data strongly suggest that the filament has become detached from both beads. For the different geometries in Figs. 1(d) and 1(f), the filament has unpinned only from the upper bead.

For the experiment in Figs. 1(a) and 1(b), we show details of the unpinning dynamics in Fig. 1(g). The time-space consists of a stack of one-dimensional intensity profiles that are collected along a vertical line positioned halfway between the two beads (perpendicular to the bead-to-bead axis). The filament loop intercepts this line twice. Because the projection of the filament into our image plane emits waves in alternating directions, the two interceptions are expected to generate two distinct fishbone-shaped patterns. During the early phase of the experiment, we indeed find two filament locations of which the right one disappears after 20 min. We suggest that this filament branch annihilated in a collision with the system boundary but it is possible that our detection merely fails to resolve it. The left filament branch is well resolved and moves in the negative y direction [i.e., downwards in Fig. 1(b)]. Its speed is high during the first 20 min, then lower, and again faster after approximately 70 min. The latter time agrees with the approximate time of detachment t_{un} from the pinning beads.

Figure 1(h) shows t_{un} as a function of the employed field strength where t_{un} is defined as the time needed to remove the vortex from at least one bead. The data suggest that the unpinning time decreases with increasing field strength. In addition, t_{un} depends on the angle ϑ between the field vector and the interbead axis. The unpinning is fastest for $\vartheta = 0$ and slowest for $\vartheta = 90^{\circ}$. Notice that we do not know

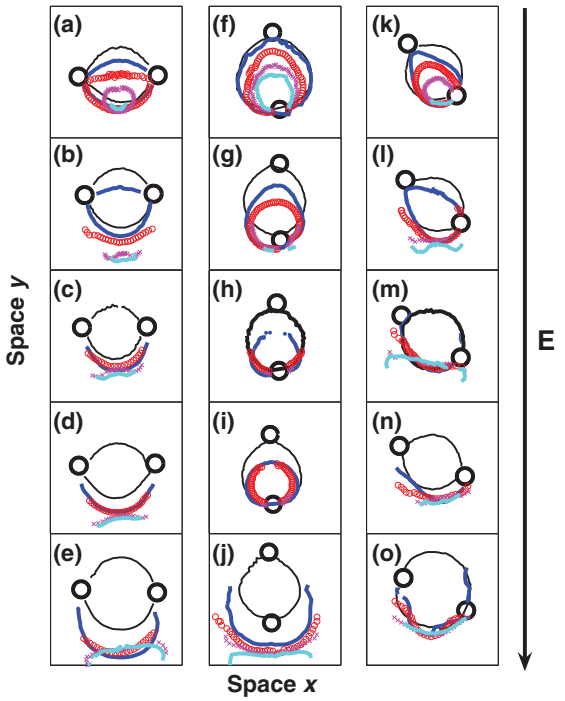

FIG. 2. (Color online) Filaments dynamics of scroll rings initially pinned to two spherical heterogeneities, in the presence of an electric field of strength (a), (f), (k) 0.5, (b), (g), (l) 1.0, (c), (h), (m) 1.5, (d), (i), (n) 2.0, and (e), (j), (o) 2.5 V/cm. The electric field vector is oriented (a)–(e) perpendicular, (f)–(j) parallel, and (k)–(o) diagonal to the line connecting the heterogeneities. Different curves correspond to different times elapsed from the start of electric field perturbation: (a–e) 5 (black, solid thin-dark line), 22 (blue, thick-dark line), 55 (red, circles), 89 (magenta, crosses), and 94 (cyan, solid thick-light line) min; (f)–(j) 5 (black, solid thin-dark line), 22 (blue, thick-dark line), 35 (red, circles), 54 (magenta, crosses), and 72 (cyan, solid thick-light line) min; (k)–(o) 5 (black, solid thin-dark line), 22 (blue, thick-dark line), 38 (red, circles), 58 (magenta, crosses), and 64 (cyan, solid thick-light line) min. The individual panels show an area of 15×15 mm^2.

whether vortex unpinning can occur for field strengths much lower than 1 V/cm. Accordingly, we currently cannot rule out the existence of a possible critical field strength E_{crit} below which vortices remain pinned. Future experiments aimed at measuring E_{crit} might be hindered by the limited lifetime of vortex states in the thermodynamically closed BZ system.

Figure 2 summarizes our results for 15 different experimental conditions. Within this panel array, the electric field strength increases from top to bottom while each column corresponds to a specific angle between the bead-to-bead axis and the field vector, which points in the negative y direction. Each subfigure illustrates the evolution of the vortex filament in terms of five color-coded curves. These data reveal that synchronous detachment from both beads occurs only if the field vector is oriented in the normal direction to the interbead axis [Figs. 2(a)–2(e)]. The field strength does not only affect the unpinning time but also the dynamics of the detached filament, which in Fig. 2(a) collapses in close vicinity of the bead pair but in Fig. 2(d) continues to move in the negative y direction with only mild contraction. In the case of electric

fields parallel to the interbead axis and $|\vec{E}| \leqslant 2.0$ V/cm [Figs. 2(f)–2(i)], the shrinking filament fails to detach from the lower bead and annihilates in its close vicinity. Only for larger fields [Fig. 2(j)], does the filament also free itself from the lower bead. In the latter case, the rapidly downward moving, left and right filament segments are most likely in contact with one of the planar system boundaries.

To obtain more detailed insights into the unpinning process, we have performed numerical simulations based on reaction-diffusion-advection equations [38] that extend the dimensionless Barkley model. The latter one is frequently used to describe excitable reaction-diffusion systems [38]. It involves two variables, u and v, which are loosely associated with the concentrations of autocatalytic species (bromous acid) and the control species of the BZ reaction (i.e., the oxidized form of ferroin and/or bromide), respectively. Following earlier studies, we model the influence of the electric field on the transport of ionic species by adding an advection term to the differential equation for the variable v. The complete model is given by

$$\frac{\partial u}{\partial t} = D_u \vec{\nabla}^2 u + \frac{1}{\epsilon} u(1-u)\left(u - \frac{v+b}{a}\right), \tag{1}$$

$$\frac{\partial v}{\partial t} = D_v \vec{\nabla}^2 v + \mu \vec{E} \vec{\nabla} v + u - v, \tag{2}$$

where the system parameters ϵ, a, and b are kept constant at 0.02, 1.1, and 0.18, respectively. The diffusion constants are $D_u = D_v = 1$. This set of parameters describes a system in which spiral waves undergo rigid rotation. Scroll waves have positive filament tension α and their binormal drift coefficient β equals zero. The drift velocity $|\mu\vec{E}|$ equals 0.05 and is the product of an ion mobility (μ) and the electric field vector ($\vec{E}$). Equations (1) and (2) are integrated using explicit Euler integration, a seven-point stencil for the Laplacian, a three-dimensional lattice measuring either $300 \times 300 \times 300$ (Figs. 3 and 4) or $300 \times 300 \times 200$ grid points (Fig. 5), and Neumann boundaries. The grid spacing and the integration time step are kept constant at 0.2 and 0.006, respectively. The pinning spheres are modeled as a region in which u and v equal zero, thus creating nearly spherical Dirichlet boundaries on the three-dimensional Cartesian grid. Their diameter is 6.0 space units and their center-to-center distance equals 26.8 space units. The filament is computed from the intersection of the waves' $u = 0.5$ and $v = a/2 - b$ surfaces using a marching-cube algorithm [39]. Three-dimensional rendering is carried out with MATLAB scripts. Notice that we also tested the unpinning from spherical heterogeneities with (more realistic) Neumann boundaries. These otherwise identical simulations yielded qualitatively the same results as our simulations with the sink-like Dirichlet boundary $(u,v) = (0,0)$ [40].

The involved advection term affects directly only the inhibitor species and models an electric field in the negative x direction. Figure 3 summarizes our findings for the case of $\vartheta = 90^\circ$ and should hence be compared to the experiments in Figs. 1(a), 1(b), 1(g), and 2(a)–2(e). The solid, orange areas in Figs. 3(a)–3(d) indicate regions of high activator concentration. The pinning beads and the filament are plotted in blue and black, respectively. Notice that we graph both beads and the entire filament; however, only the posterior half of the wave pattern is shown as the entire structure is

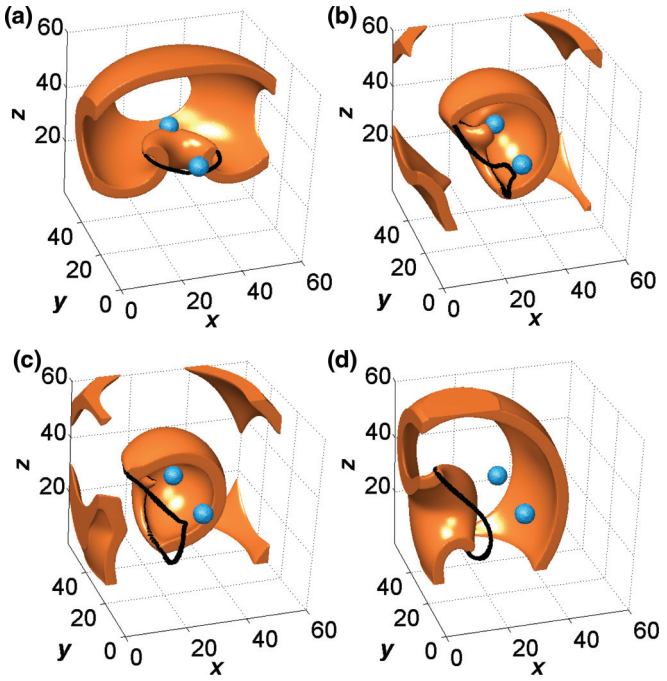

FIG. 3. (Color online) Simulation of the unpinning of a scroll wave in a three-dimensional reaction-diffusion-advection model. The image sequence shows only the posterior half of the vortex field (orange) u. The pinning spheres are rendered in cyan and the filament is plotted as a black curve. The homogenous, constant electric field is oriented in the negative x direction.

symmetric with respect to the plane given by $y = 30$. The initially circular filament [Fig. 3(a)] remains pinned while the loop turns perpendicular to the field vector [Fig. 3(b)] and is pulled in the negative x direction. During this phase, the filament has the strongest out-of-plane deformations, which are mainly caused by the cusp-like segments that connect the main loop plane to the beads. Around the time of snapshot of Fig. 3(c), the filament detaches from the beads. The now free cusps have a high curvature and hence move quickly in the

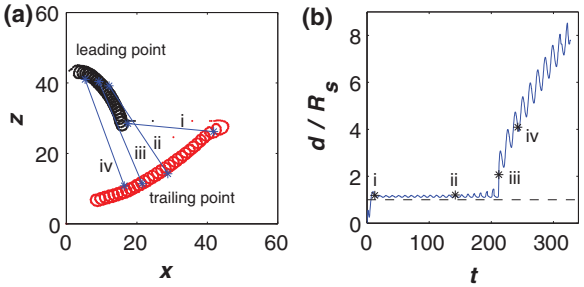

FIG. 4. (Color online) Analysis of the unpinning dynamics for the example shown in Fig. (3). (a) Trajectories of the leading and trailing points of the filament. The coordinate pairs (stars) for the times in Figs. 3(a)–3(d) are labeled as "i" to "iv," respectively, and are connected by blue lines to indicate the approximate tilt angle of the filament loop. (b) Shortest distance between the filament loop and the centers of the pinning bead as a function of time. The distance is shown as multiples of the bead radius R_s (dashed line at $d/R_s = 1$). The times shown in Figs. 3(a)–3(d) are again labeled as "i" to "iv," respectively.

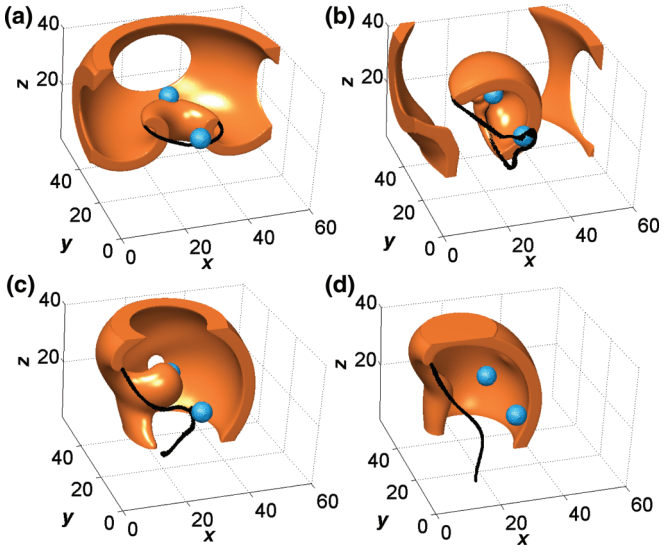

FIG. 5. (Color online) Simulation of the unpinning of a scroll wave in system for which the height in the z direction is one-third smaller than in Fig. 3. (a)–(d) Image sequence illustrating the key stages of the unpinning process. Only the posterior half of the vortex field (orange) is shown. The pinning spheres are rendered in cyan and the filament is plotted as a black curve. The homogenous, constant electric field is oriented in the negative x direction.

direction of the main loop. The less deformed, free filament in Fig. 3(d) then continues to move toward the left system boundary where it eventually annihilates.

The tilting of the loop is also illustrated in Fig. 4(a), where we trace the leading (smallest x value) and trailing points (largest x) of the filament. The unpinning event (see the connecting line labeled "iii" does not cause a discontinuous or otherwise noteworthy change in the trajectories. However, the temporal evolution of shortest distance d between the filament and any of the two bead centers reveals that the unpinning of the scroll wave is an abrupt and not a gradual process [Fig. 4(b)]. In this simulation unpinning occurs after 210 time units or the equivalent of about 21 rotation cycles.

As mentioned earlier, our experimental results are not fully conclusive as to the fate of the lower filament branch. It is possible that the lower part of the filament loop collides with the lower system boundary during the initial tilting process. We have hence performed numerical simulations in a 33% thinner system measuring $300 \times 300 \times 200$ grid points. All other parameters, constraints, and initial conditions are identical to the simulation results shown in Fig. 3. Figure 5 illustrates the results obtained from such computations. Our results indicate that the filament-wall collision, which occurs around $t = 175$, does not affect the unpinning time significantly.

IV. CONCLUSIONS

Our study demonstrates that pinned scroll waves can be removed from their anchoring heterogeneities by external fields that induce electromigration or similar advective perturbations. Experiments and simulations show that the unpinning process is not instantaneous but that it involves a large-scale reorientation of the vortex loop. One can speculate that a larger number of pinning sites or more extended anchor regions, such as cylindrical objects, should further delay or possibly prevent unpinning. The results also reveal that the detachment of a filament pinned to several anchors occurs sequentially. In highly heterogeneous systems such behavior should give rise to alternating sequences of slow reorientation dynamics and rather sudden unpinning events. Furthermore, it seems possible that these processes could cause single filament loops to split into two or more loops.

We also showed that the unpinned filaments have highly curved, cusp-like features [Fig. 3(c)]. These cusps resulted from two, initially separate filaments that locally can be considered independent (unconnected) curves. We suggest that such a filament pair can unpin only if it fulfills the following necessary conditions: (i) sufficiently small interfilament distance and (ii) opposite chirality. The latter is necessary for ensuring a unique direction of scroll rotation along the entire newly formed curve.

Condition (i) is reminiscent of recent results that revealed the existence of filament repulsion for distances much shorter than the vortex wavelength and filament attraction at even shorter distances [32,41]. This attraction appears to be the essential component of the observed unpinning processes. Accordingly, a very short segment of the filament pair might annihilate in close vicinity of the pinning sphere, thus liberating the now continuous curve. We further suggest that the details of this process are closely related to filament reconnections in cross-over collisions [42,43].

While our experiments and simulations study intrinsically isotropic systems, it seems likely that similar phenomena must occur in cardiac tissue. If reentrant waves in the heart have the potential to pin to heterogeneities such as remodeled myocardium, papillary muscle insertion points, and blood vessels, knowledge about the stability of these states against intrinsic factors as well as external intervention strategies [18,44] are of importance. Clearly much remains to be learned regarding the physics of pinned vortex states in excitable media and their relevance in living systems.

ACKNOWLEDGMENT

This material is based upon work supported by the National Science Foundation under Grant No. 1213259.

[1] L. Glass, Nature **410**, 277 (2001).
[2] J. S. O'Neill *et al.*, Nature **469**, 554 (2011).
[3] O. Wartlick, P. Mumcu, F. Jülicher, and M. Gonzalez-Gaitan, Nat. Rev. Mol. Cell Biol. **12**, 594 (2011).
[4] G. Buzsáki and A. Draguhn, Science **304**, 1926 (2004).
[5] J. Krupic, N. Burgess, and J. O'Keefe, Science **337**, 853 (2012).
[6] S. Luther *et al.*, Nature **475**, 235 (2011).
[7] R. D. Traub and R. K. Wong, Science **216**, 745 (1982).
[8] F. H. Fenton, E. M. Cherry, H. M. Hastings, and S. J. Evans, Chaos **12**, 852 (2002).

[9] S. V. Pandit and J. Jalife, Circ. Res. **112**, 849 (2013).
[10] J. M. Davidenko, A. V. Pertsov, R. Salomonsz, W. Baxter, and J. Jalife, Nature **355**, 349 (1992).
[11] A. T. Winfree, Science **266**, 1003 (1994).
[12] J. Jalife, Ann. Rev. Physiol. **62**, 25 (2000).
[13] J. N. Weiss, Z. Qu, P.-S. Chen, S.-F. Lin, H. S. Karagueuzian, H. Hayashi, A. Garfinkel, and A. Karma, Circulation **112**, 1232 (2005).
[14] H. Dierckx, H. Verschelde, O. Selsil, and V. N. Biktashev, Phys. Rev. Lett. **109**, 174102 (2012).
[15] P. Dähmlow, S. Alonso, M. Bär, and M. J. B. Hauser, Phys. Rev. Lett. **110**, 234102 (2013).
[16] J. P. Keener and J. J. Tyson, SIAM Rev. **34**, 1 (1992).
[17] V. N. Biktashev, A. V. Holden, and H. Zhang, Philos. Trans. Roy. Soc. A **347**, 611 (1994).
[18] S. Alonso, F. Sagues, and A. S. Mikhailov, Science **299**, 1722 (2003).
[19] T. Bánsági, Jr. and O. Steinbock, Phys. Rev. Lett. **97**, 198301 (2006).
[20] O. Steinbock, F. Siegert, C. J. Weijer, and S. C. Müller, Proc. Natl. Acad. Sci. USA **90**, 7332 (1993).
[21] A. T. Winfree, Science **181**, 937 (1973).
[22] L. D. Weise and A. V. Panfilov, Phys. Rev. Lett. **108**, 228104 (2012).
[23] Y. Zhang *et al*., Soft Matter **8**, 7056 (2012).
[24] Y. Sun, Cardiovasc. Res. **81**, 482 (2009).
[25] S. Zlochiver *et al*., Biophys. J. **95**, 4469 (2008).
[26] I. D. Greener *et al*., J. Am. Coll. Cardiol. **60**, 1103 (2012).
[27] O. Steinbock and S. C. Müller, Physica A **188**, 61 (1992)
[28] V. Zykov, G. Bordyugov, H. Lentz, and H. Engel, Physica D **239**, 797 (2010).
[29] Z. A. Jiménez and O. Steinbock, Phys. Rev. E **86**, 036205 (2012).
[30] Z. A. Jiménez, B. Marts, and O. Steinbock, Phys. Rev. Lett. **102**, 244101 (2009).
[31] Z. A. Jiménez and O. Steinbock, Europhys. Lett. **91**, 50002 (2010).
[32] Z. A. Jiménez and O. Steinbock, Phys. Rev. Lett. **109**, 098301 (2012).
[33] A. V. Panfilov and A. N. Rudenko, Physica D **28**, 215 (1987).
[34] O. Steinbock, J. Schütze, and S. C. Müller, Phys. Rev. Lett. **68**, 248 (1992).
[35] J. Schütze, O. Steinbock, and S. C. Müller, Nature **356**, 45 (1992).
[36] M. Vinson, S. Mironov, S. Mulvey, and A. Pertsov, Nature **386**, 477 (1997).
[37] C. Luengviriya, S. C. Müller, and M. J. B. Hauser, Phys. Rev. E **77**, 015201 (2008).
[38] D. Barkley, Physica D **49**, 61 (1991).
[39] M. Dowle, R. M. Mantel, and D. Barkley, Int. J. Bifurcation Chaos **7**, 2529 (1997).
[40] See Supplemental Material at http://link.aps.org/supplemental/10.1103/PhysRevE.88.052918 for numerical simulation of scroll ring unpinning from Neumann boundaries.
[41] M. A. Bray and J. P. Wikswo, Phys. Rev. Lett. **90**, 238303 (2003).
[42] M. Gabbay, E. Ott, and P. N. Guzdar, Phys. Rev. E **58**, 2576 (1998).
[43] B. Fiedler and R. M. Mantel, Documenta Math. **5**, 695 (2000).
[44] M. Horning, S. Takagi, and K. Yoshikawa, Phys. Rev. E **85**, 061906 (2012).